On the Benefits of Ray-Based Modeling for Analyzing On-Body MmWave Systems

Aleksei Ponomarenko-Timofeev*, Olga Galinina*, Andrey Turlikov†, and Sergey Andreev*
*Tampere University, Finland
{aleksei.ponomarenko-timofeev, olga.galinina, sergey.andreev}@tuni.fi
†State University of Aerospace Instrumentation, Russia
turlikov@vu.spb.ru

***Abstract*—While optimizing the system-level performance in a network of advanced high-end wearables, millimeter-wave (mmWave) medium access protocols may benefit from leveraging the information on the spatial and temporal dynamics of the radio channel. In this paper, we aim to bridge the existing gap in mmWave on-body propagation studies by analyzing the channel structure based on an extensive shooting-and-bouncing ray (SBR) simulations. Particularly, we model a set of on-body trajectories and illustrate the evolution of the core channel parameters as well as address the specifics of their dynamics, which can be exploited in further protocol development. As a key contribution of this study, we propose a methodology for processing and applying the simulation data as well as illustrate our approach through an example of estimating the effects of directionality and antenna beam misalignment. Our results and data, also available online, facilitate the system-level analysis and performance evaluation of various on-body mmWave systems.**

***Index Terms*—mmWave comunications, on-body propagation, ray-based modeling, directionality, performance evaluation, system analysis.**

I. Introduction

As increasing numbers of high-end eyewear devices (e.g., AR/VR glasses) are flooding the consumer market, it is becoming clear that conventional microwave technologies may be unable to support their reliable connectivity on the level required to satisfy the stringent quality-of-experience demands. Consequently, one of the key enablers for standalone operation of such advanced wearables may be sought in a much wider millimeter wave (mmWave) spectrum. Both academic and industrial communities have thus geared their research efforts towards exploring cellular and local area mmWave networks that rely on medium/long-range links, while short-range mmWave communications have received relatively scarce attention.

In the case of on-body mmWave communications – for example, when a wearable device offloads demanding computations and processing to a personal access point – the radio channel exhibits considerably different properties compared to long-range communications. This fact can be effectively exploited to improve the overall system performance by adjusting PHY and MAC protocols to the specifics of on-body mmWave channels. The protocol development walks hand in hand with thorough system-level modeling and performance evaluation to capture the effects, e.g., of complex human mobility patterns and, therefore, calls for a deeper understanding of the underlying on-body channel structure.

One approach to explore the channel parameters is the use of the finite-difference time-domain (FDTD) method, which is based on discretizing the time-dependent Maxwell's equations and solving the corresponding finite-difference equations; however, its applicability is limited due to demanding memory and CPU load. For example, one of the requirements to maintain the numerical stability of the FDTD calculations is that the considered model should be divided into cells having dimensions that are much smaller than the wavelength. For the unlicensed carrier frequency of 60 GHz, it translates to dimensions of 1.25 mm at most; thus, the memory usage grows unacceptably fast with the frequency and scenario scale, which substantially limits the applicability of the method. Conveniently, the wavelength in the extreme high frequency (EHF) spectrum allows applying shooting-and-bouncing ray (SBR) methods; however, the computation intensity renders this approach infeasible in the case of extensive system-level simulations.

Another possible way to model the radio channel is by pre-generating a fading map that will be utilized further in simulations [1]. This approach can be used in multiple scenarios with static obstacles that are smaller compared to the wavelength as it provides a computationally lighter solution to estimating the channel parameters. While this approach offers accurate results for microwave networks, it might become infeasible for mmWave systems.

In this regard, there is a need for an in-depth analysis of mmWave on-body channel dynamics and development of computationally light models, which reproduce the propagation parameters and potentially embrace complex effects of human body geometry and motion (including mobility of limbs and breathing), which is characteristic of future 5G/5G+ mobile XR applications.

In this paper, we aim to bridge the existing gap in exploring the dynamics of the mmWave on-body signal propagation and analyze the radio channel structure by using extensive SBR simulations. The contributions of this paper are as follows:

- We model a set of on-body antenna trajectories covering a human body. For these trajectories, we illustrate the evolution of the core channel parameters, such as power, phase, delay, and angular information, as well as address the specifics of their dynamics and structure that can be exploited further in protocol development.

- We propose a methodology of processing the obtained ray-based data and offer a detailed instruction on the use of the estimated channel information in the system-level analysis. Particularly, we provide an illustrative example of assessing the effects of directionality and antenna beam misalignment for link- and system-level simulation studies.
- Finally, we make all presented data and underlying processing scripts accessible online so that they can either be reused directly for further mmWave system-level studies or serve as a basis for deriving spatially-consistent on-body channel models suited for beyond-5G wearable systems.

The remainder of this paper is structured as follows. Section II provides a brief description of the mmWave channel modeling landscape. In Section III, we describe our simulation environment and scenarios of interest. In Section IV, we illustrate the structure of the mmWave on-body channel in terms of the received power, angular, phase, and delay information. Finally, in Section V, we draw our conclusions on the structure of the mmWave on-body channel and outline potential directions for development. In addition, we share all our results in BitBucket [2] along with the post-processing Octave scripts.

II. Background on mmWave On-Body Modeling

While microwave network simulation and planning may benefit from applying convenient statistical models, such as Okumura-Hata and COST-231, mmWave on-body channels have a more complex structure, and therefore the use of similar models (mostly built for large-scale scenarios) might cause significant inaccuracy. The two-ray model may also appear insufficiently detailed for the analysis of on-body links due to the presence of strong multipath components, which are caused by mobility and reflections from the complex geometry of the human body or its surrounding environment.

For the mmWave frequencies, the research community has produced a large number of propagation models that cover various indoor, outdoor, and outdoor-to-indoor scenarios [3]–[7] as well as explore multiple-input-multiple-output (MIMO) systems by providing detailed results on the power, antenna polarization, and angular information [8], [9]. While these studies mainly focus on large- and medium-scale scenarios (both in licensed and unlicensed bands), body area networks receive considerably less attention.

In body area networks, channel parameter values can be sensitive to even minor changes in the environment [10], [11]. For example, breathing movements have a certain impact on the received power and delay [12], while the body surface affects the angle of arrival [13]. To this end, the nature of the short-range mmWave links calls for new modeling criteria that would define a class of models suitable for further system-level analysis and evaluation of mmWave on-body systems.

A specific set of requirements for mmWave statistical models has been defined by the 802.11ay task group [14]. Particularly, the models should be capable of maintaining spatial consistency in terms of, e.g., phase, power, and angular information. An example of a geometry-based stochastic model having spatial consistency can be found in [15]; however, this model does not support small-scale scenarios and, therefore, cannot be directly applicable to on-body mmWave links. To the best of our knowledge, the only model addressing the small-scale mobility of wearable devices is provided in [16]; specifically, it emulates a walking user and employs the data produced by simulating multiple off-body scenarios.

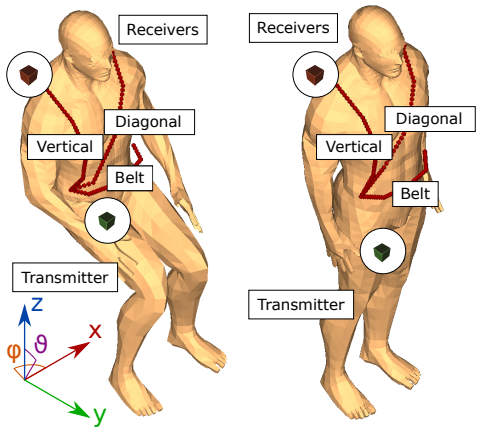

(a) Sitting posture. (b) Standing posture.

Fig. 1: 3D models of human body, elevation ϑ, azimuth ϕ.

III. Methodology, Modeling Tools, and Scenarios

A. Modeling environment and configuration

We model an on-body scenario in RemCom Wireless InSite software package [17] and derive the total received power, channel impulse response (CIR), and angular data (arrival/departure angles) using the integrated SBR method. As we focus on the on-body propagation, we capture signal interactions using rigged 3D mesh of the human body and filter out the paths reflected from the surroundings (can be added separately, due to the superposition property). A detailed configuration of the receiver and transmitter antennas in the simulation engine can be found in Table I.

TABLE I: Receiver/transmitter configuration.

Parameter	Value
Antenna	Isotropic
Antenna Gain	0 [dBi]
TX Power	0 [dBm]
Polarization	Vertical [rel. to ground]
Waveform	Sinusoidal
Frequency	60 [GHz]
Noise figure	3 [dB]
Initial phase	0 [deg]

Further, we reproduce detailed 3D models of the human body (depicted in Fig. 1), which consist of approximately 1000 triangles each, by carefully customizing them in Blender to decrease the simulation time and achieve stable results. In particular, less detailed models produce inconclusive data since

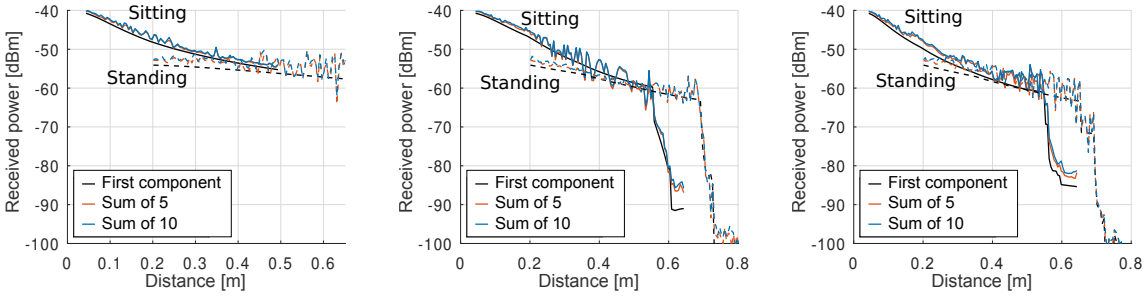

(a) Belt trajectory. (b) Vertical trajectory. (c) Diagonal trajectory.

Fig. 2: Rx power evolution for three trajectories and two scenarios: dashed (solid) lines correspond to standing (sitting) position.

the degree of detail affects how the signal travels through the simulation environment. Increasing the polygon count further yields little to no difference in the channel parameters, while the simulation time increases substantially. Consequently, the modeled scenario should maintain an appropriate level of detail (LOD), which can be estimated by gradually decreasing the number of polygons until notable changes in the channel image appear, caused by the change in positions and orientations of reflectors and scatterers. Due to the constraints of the integrated method, we also limit our 3D models by the minimum size of an individual face element, which has to exceed 4λ, where λ is the wavelength.

In addition to 3D geometry settings, it is also important to configure the Wireless InSite engine to minimize the time of computation and maintain the required precision of the results. The detailed parameters of the engine are given in Table II.

TABLE II: X3D SBR parameters.

Parameter	Value
Ray spacing	0.05°
Maximum number of penetrations	2
Maximum number of reflections	4
Maximum number of diffractions	1
Diffuse scattering	Disabled
Noise floor	-160 dBm
Number of stored paths	250
Ambient temperature	20.0° [C]

B. Scenarios and general methodology

We study two distinct scenarios: replicating sitting and standing human positions, as shown in Fig. 1. For each scenario, three receiver trajectories are considered: (i) vertical upward trajectory, (ii) diagonal upward trajectory, and (iii) trajectory in front of the belt. The receivers are separated from the body by a constant offset so that the trajectory is conformal to the body surface. Therefore, the trajectories mimic locations of high-rate and low-latency consumer devices, such as an on-body camera or medical equipment. The spacing between neighboring receiver positions is set to one wavelength. The transmitter is always located at the pocket level representing the location of a smartphone or another personal access point; its precise coordinates vary due to different leg positions for the sitting and standing cases. Importantly, each trajectory may also illustrate a potential movement of the device along the human body (vertically, horizontally, or diagonally) and, thus, sheds light on the temporal dynamics of the measured parameters.

We explore a total of six different sets of receiver-transmitter (RX/TX) links so that for each pair in a set, we initially calculate 250 multipath components (sorted in descending order). For each modeled multipath component, we extract the phase, received power, delay, and angular information. To define the number of propagation paths sufficient for collecting the total received power, we explore changes in the power as the number of components increases. To correctly handle the phase information, we calculate the total received power through the complex amplitude:

$$A_i = e^{-1j\cdot\phi_i} \cdot \sqrt{10^{P_i/10}}, \tag{1}$$

where i is the index of the propagation path, ϕ_i is the phase of the signal arriving over path i, and P_i is the power in dBm delivered over path i.

When we double the number of summed up components from five to ten, as shown in Fig. 2, the total received power does not experience any significant change; however, it occasionally drops below the power of the first component. This can be explained by the fact that some of the multipath components arrive in counter-phase and attenuate each other, thus decreasing the total received power. We further refer to the power data that contain the first five components. A general scheme of our methodology is provided in Fig. 3.

In Fig. 2, one may also notice a self-blockage event that occurs on the vertical and diagonal trajectories at 100th receiver position, contrary to the belt trajectory. We may further observe how the presence of reflections from legs increases the total received power irrespectively of the trajectory direction. Particularly, the received signal power is higher for the sitting position than that in the standing case, which can be explained by the fact that legs act as reflectors for a sitting person.

Importantly, the core behavior of the channel image does not vary significantly across the trajectories. Consequently, for the sake of brevity, we continue with analyzing one selected trajectory, e.g., the vertical case of the sitting position scenario. The full set of results can be found in our repository [2].

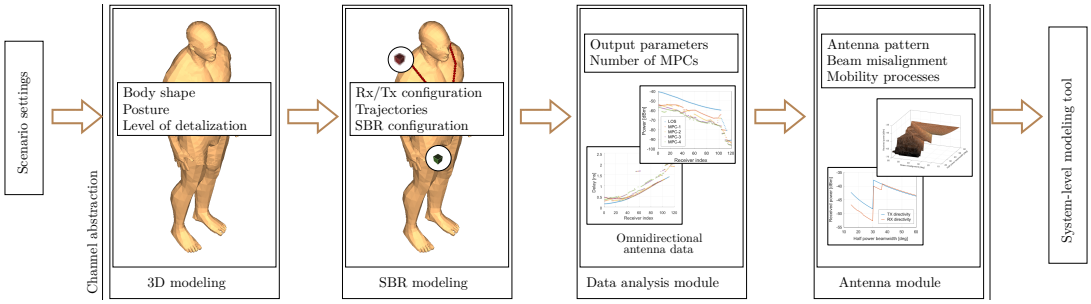

Fig. 3: Illustration of our proposed workflow.

C. Application of directional antenna patterns

The information on the phase, power, and elevation/departure angles can be exploited to apply any desired antenna pattern at the receiver and/or transmitter for calculating the total received power in further system-level analysis. To illustrate the application of directional antenna patterns to the data set of the proposed structure, we introduce the following assumptions.

We approximate our theoretical directional antenna pattern by a cone of the apex angle θ, where θ represents a half-power beamwidth (HPBW), and assume a perfect antenna alignment for each RX/TX pair. The cone axis is directed along the strongest multipath, which could be a result of complex beamforming procedures. We note that if the system model assumes an imperfect alignment, the corresponding offset may be introduced as a random variable with a certain distribution that can be deduced, e.g., from the mobility pattern and beamforming frequency.

To reuse the omnidirectional data set, we update the channel information by excluding all rays that arrive outside the cone with the azimuth and elevation deviating from the axes (antenna boresight) more than 0.5θ. Importantly, one may easily incorporate any 3D shape of the antenna pattern, where the power of a particular ray is adjusted according to the respective directivity gain value in that direction. For better tractability of these results, we further continue with the conic shape assumption, without loss in generality.

To estimate the directivity effects we assume a sector pattern of the antenna, which is a coarse approximation of cone antenna, whose directivity gain is monotonically decreasing with respect to the beamwidth and can be approximated by the following ratio based on the expression for a solid angle:

$$G[\text{dB}] = 10\log_{10}\left(\frac{2}{1-\cos\frac{\theta}{2}}\right), \tag{2}$$

where θ is the beamwidth.

In our scenario, the received power after the described filtration might drop for many locations, especially when the line-of-sight (LOS) link is lost after the receiver travels behind the shoulder. A simplified example of filtering is given in Fig. 4, where paths 2, 3, and 4 experience reflections from the reflecting surfaces, and path 1 is the LOS. In this example, rays 1, 2, and 3 are received normally for our antenna directivity

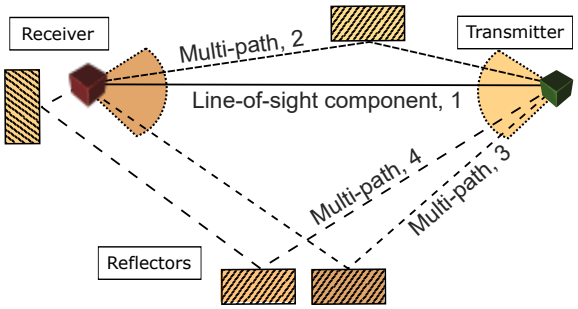

Fig. 4: Example of angular ray filtration.

abstraction; however, ray 4 is ignored, being isolated by the antenna pattern at the receiver.

Importantly, this approach illustrates how the data of the proposed structure can be helpful in simulating (highly) directional transmission using the isotropic antenna data. Examples demonstrating the proposed methodology are addressed in the following section.

IV. Numerical Analysis

Here, we provide selected numerical results for the scenario that corresponds to the vertical trajectory along the body of a sitting human. We emphasize that the goal of this example case is to streamline the discussion since the structure of the presented data remains similar across all six scenarios. We split our numerical analysis into two parts: the first one contains insights into the dynamics of the computed channel parameters, while the second part offers an example of applying a directional antenna pattern to the omnidirectional data set for estimating the effects of the antenna beam misalignment. We note that an alternative approach based on measurement data would be seriously constrained if not impossible since most of the information is not accessible to measure, and even rough estimation requires cumbersome adjustment of sector sweep procedures.

A. Analysis of channel structure

For the vertical trajectory of a sitting human, we export power, delay, phase, and angular information for five paths as justified in subsection III.C. The respective data are illustrated in Fig. 5, 6, and 7, where the blue color corresponds to the first multipath, and other colors stand for the rest four individual components sorted in descending order of the received power.

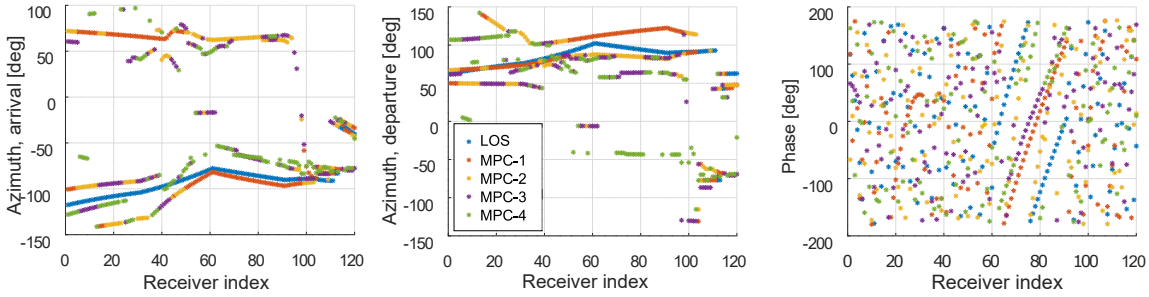

(a) Arrival azimuth. (b) Departure azimuth. (c) Phase.

Fig. 5: Azimuth and phase for 5 dominant components in vertical trajectory of sitting model.

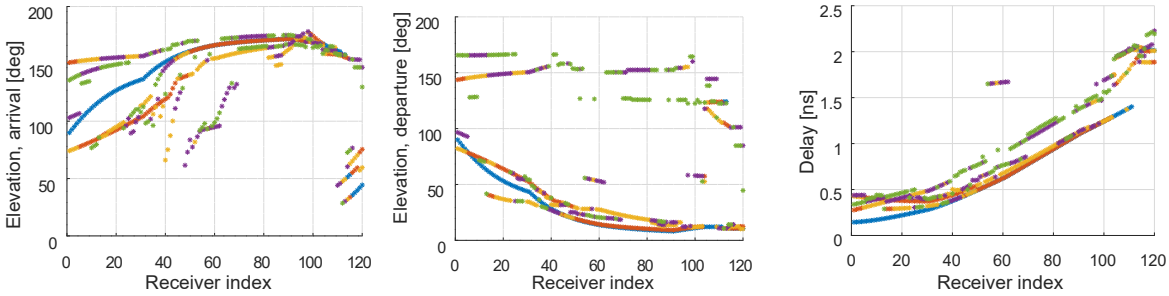

(a) Arrival elevation. (b) Departure elevation. (c) Arrival delay.

Fig. 6: Elevation and delay for 5 dominant components in vertical trajectory of sitting model.

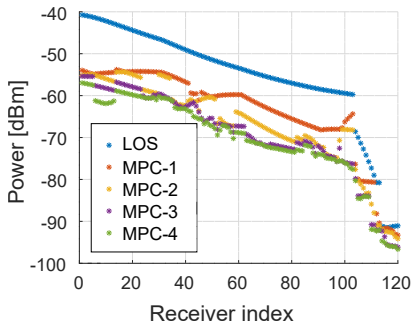

Fig. 7: Received power of individual components.

We intentionally reproduce the varied receiver index; however, it can be trivially mapped onto the distance without changes in the shape of the trajectories. The phase and the power of the individual components can be directly derived from the delay (see Fig. 5c, 6c, and 7), if the component corresponds to a LOS link. This can be explained by the fact that if there are no reflectors/diffractors in the propagation path, the phase depends only on the time of flight. Otherwise, if a propagation path contains any reflection, transmission, or diffraction events, neither the received power nor the phase can be restored from the delay information. This is because each interaction with the environment will change the characteristics of the signal arriving over a specific path.

Importantly, all data in Fig. 5, 6, and 7, except for the phase, demonstrate similar visual structure. The detected multipath components form visibly continuous trajectories while moving from the receiver position 1 to 120. Given a number of similar sets, one may construct a statistical model able to generate random trajectories of a given structure, which naturally preserve spatial consistency due to the continuity of the curves.

B. Impact of antenna beamwidth

Here, we illustrate our approach to applying a theoretical directional antenna pattern as described in subsection III.C by an example of a cone approximation, where the antenna beamwidth θ and beam misalignment $\Delta\theta$ are swept over $10°$–$60°$ range. Specifically, Fig. 8 shows the impact of the HPBW and beam misalignment $\Delta\theta$ on the total received power for a specific selected position. Here, we may observe a situation where a secondary path enters the transmission sector at HPBW of $35°$ and misalignment of $60°$.

The sub-figure in the top-right corner of Fig. 8 depicts the 2D cross-section of the surface plot for both receiver and transmitter directivity. In this particular case, the antenna pattern is offset by a fixed value $\Delta\theta = 30°$ from the dominant ray (by both azimuth and elevation) representing the beam misalignment. As the HPBW reaches the offset value of $\Delta\theta$, the received power abruptly increases to its maximum. Interestingly, the angular filtration yields dissimilar results for the transmit and receive antennas, which can be explained by the fact that the LOS and non-LOS (NLOS) are reflected from the surface behind the transmitter. If we apply an angular filter, similar to the one we use, we may observe two components at the receiver; however, the same filter at the transmitter antenna eliminates the NLOS path, as discussed in subsection III.C.

In practice, the use of narrow beam antennas might appear financially infeasible for some devices, resulting in lower antenna gains and potentially lower rates and higher delays

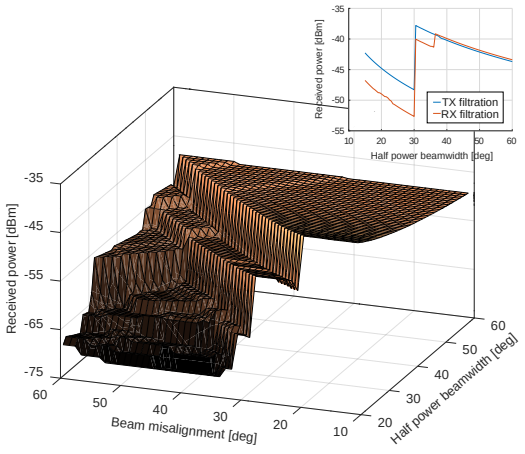

Fig. 8: Power vs. different TX misalignment and HPBW.

due to frequent antenna configuration updates. Depending on the intensity and scale of the body mobility as well as the temporal characteristics of the beam misalignment process, wider beams may result in higher received power, which adds new dimensions to the commonly known directionality trade-off of mobility, gain, and beam training overhead.

V. Conclusions

In this paper, we model the mmWave channel for six characteristic on-body scenarios, which are driven by the mass adoption of rate-demanding wearable applications. We emphasize that the presence of multiple external reflectors in the user proximity does not obviate the need to rely on on-body links. The electromagnetic properties of reflectors highly depend on the environment conditions (humidity, precipitation, and foliage) and cannot be controlled by the body area network. This may hinder the operation through external reflections, making on-body links, in some circumstances, the only viable option to rely upon.

Our proposed methodology for ray-based data processing and system analysis covers the nature of directional transmission systems and is illustrated by selected numerical examples. Particularly, we estimate the impact of directional antenna misalignment in terms of the received power in the case of lower angular resolution. In our example, increasing the antenna HPBW from 15° to 30° may result in approximately 10 dB gain in the received power. We may conclude that narrow-beam antennas might not always lead to higher signal power and better channel conditions if the communicating devices are highly mobile. The temporal characteristics of the mmWave channel exhibit strong spatial correlation and thus may produce predictor models for power, delay, and angular information.

The results of our paper, also available online [2], may be used as follows: (i) directly in the link- and system-level analysis, (ii) when applying the antenna directivity and exploring the impact of antenna patterns and various stochastic processes generating beam misalignment degree, and (iii) for constructing predictive models based on regenerating the data of similar continuous-curve structure, for a range of input parameters.

VI. Acknowledgments

The research of A. Turlikov was supported by the Russian Science Foundation (project no. 18-19-00673). The work of O. Galinina is supported by the Academy of Finland (project CROWN).

References

[1] H. Claussen, "Efficient modelling of channel maps with correlated shadow fading in mobile radio systems," in *PIMRC*, vol. 1, pp. 512–516, 2005.

[2] A. Ponomarenko-Timofeev, "BitBucket repository with PHY layer simulation results and post-processing scripts." https://bitbucket.org/Ponomarenko-Timofeev/sbrresults/, 2020.

[3] ETSI, "3GPP TR 39.901, Release 14: Study on channel model for frequencies from 0.5 to 100 GHz," January 2018.

[4] A. Karttunen, A. F. Molisch, S. Hur, J. Park, and C. J. Zhang, "Spatially consistent street-by-street path loss model for 28-GHz channels in micro cell urban environments," *IEEE Transactions on Wireless Communications*, vol. 16, no. 11, pp. 7538–7550, 2017.

[5] A. Chandra, A. U. Rahman, U. Ghosh, J. A. García-Naya, A. Prokeš, J. Blumenstein, and C. F. Mecklenbräuker, "60-GHz Millimeter-Wave Propagation Inside Bus: Measurement, Modeling, Simulation, and Performance Analysis," *IEEE Access*, vol. 7, pp. 97815–97826, 2019.

[6] K. Haneda, J. Zhang, L. Tan, G. Liu, Y. Zheng, H. Asplund, J. Li, Y. Wang, D. Steer, C. Li, T. Balercia, S. Lee, Y. Kim, A. Ghosh, T. Thomas, T. Nakamura, Y. Kakishima, T. Imai, H. Papadopoulos, T. S. Rappaport, G. R. MacCartney, M. K. Samimi, S. Sun, O. Koymen, S. Hur, J. Park, C. Zhang, E. Mellios, A. F. Molisch, S. S. Ghassamzadeh, and A. Ghosh, "5G 3GPP-Like Channel Models for Outdoor Urban Microcellular and Macrocellular Environments," in *2016 IEEE 83rd Vehicular Technology Conference (VTC Spring)*, pp. 1–7, May 2016.

[7] T. S. Rappaport, Y. Xing, G. R. MacCartney, A. F. Molisch, E. Mellios, and J. Zhang, "Overview of millimeter wave communications for fifth-generation (5G) wireless networks—with a focus on propagation models," *IEEE Transactions on Antennas and Propagation*, vol. 65, pp. 6213–6230, Dec 2017.

[8] L. Liu, C. Oestges, J. Poutanen, K. Haneda, P. Vainikainen, F. Quitin, F. Tufvesson, and P. De Doncker, "The COST 2100 MIMO channel model," *IEEE Wireless Communications*, vol. 19, no. 6, pp. 92–99, 2012.

[9] D. He, L. Wang, K. Guan, B. Ai, J. Kim, and Z. Zhong, "Channel characterization for mmWave vehicle-to-infrastructure communications in urban street environment," in *2019 13th European Conference on Antennas and Propagation (EuCAP)*, pp. 1–5, March 2019.

[10] K. Venugopal and R. W. Heath, "Location based performance model for indoor mmWave wearable communication," in *2016 IEEE International Conference on Communications (ICC)*, pp. 1–6, IEEE, 2016.

[11] T. Bai and R. W. Heath, "Analysis of self-body blocking effects in millimeter wave cellular networks," in *2014 48th Asilomar conference on signals, systems and computers*, pp. 1921–1925, IEEE, 2014.

[12] T. Kumpuniemi, M. Hämäläinen, K. Y. Yazdandoost, and I. Jari, "Measurements for body-to-body UWB WBAN radio channels," in *2015 9th European Conference on Antennas and Propagation (EuCAP)*, pp. 1–5, IEEE, 2015.

[13] T. Wu, T. S. Rappaport, and C. M. Collins, "The human body and millimeter-wave wireless communication systems: Interactions and implications," in *2015 IEEE International Conference on Communications (ICC)*, pp. 2423–2429, IEEE, 2015.

[14] "Channel Models for IEEE 802.11ay." https://mentor.ieee.org/802.11/dcn/15/11-15-1150-09-00ay-channel-models-for-ieee-802-11ay.docx. Accessed 17.08.2019.

[15] V. Nurmela and P. Kyosti, "A spatially consistent radio channel model enabling dual mobility," in *2014 IEEE 80th Vehicular Technology Conference (VTC2014-Fall)*, pp. 1–5, IEEE, 2014.

[16] K. Turbic, L. M. Correia, and M. Beko, "A mobility model for wearable antennas on dynamic users," *IEEE Access*, vol. 6, pp. 63635–63648, 2018.

[17] RemCom Incorporated, "RemCom wireless insite software." https://www.remcom.com/wireless-insite-em-propagation-software.